TUTORIAL REVIEW

Mechanical chiral resolution

Vincent Marichez,[a] Alessandra Tassoni,[a] Robert P. Cameron,[b] Stephen M. Barnett,[c] Ralf Eichhorn,[d] Cyriaque Genet,[a] and Thomas M. Hermans*[,a]

Received 00th January 20xx,
Accepted 00th January 20xx

DOI: 10.1039/x0xx00000x

Mechanical interactions of chiral objects with their environment are well-established at the macroscale, like a propeller on a plane or a rudder on a boat. At the colloidal scale and smaller, however, such interactions are often not considered or deemed irrelevant due to Brownian motion. As we will show in this tutorial review, mechanical interactions do have significant effects on chiral objects at all scales, and can be induced using shearing surfaces, collisions with walls or repetitive microstructures, fluid flows, or by applying electrical or optical forces. Achieving chiral resolution by mechanical means is very promising in the field of soft matter and to industry, but has not received much attention so far.

1 Introduction

The first reference to chirality traces back to 360 BC and is attributed to Plato in his discussion with peers about the vision mechanism.[1] More than two millennia later this notion was revisited by young Louis Pasteur who identified "handed-molecules",[2] based on previous work by Fresnel[3] on circularly polarized light. Molecules that could not be superposed with their respective mirror images were found to have the unique ability to rotate the plane of polarized light and were thus said to display optical activity, at that time denoted as “dissymmetry”. Pasteur’s attribution of the latter effect to the three-dimensional arrangement of atoms in molecules was later confirmed by Le Bel[4] and independently by van ’t Hoff[5]. However, since dissymmetric objects were not necessarily asymmetric, the word “dissymmetry” (although still widely used in France) was slowly replaced by “chirality” as put forward by Lord Kelvin[6].

Life is chiral, and most biological processes found in nature are stereospecific, i.e. sensitive to the handedness of the molecules involved. As a result, most drugs must be administrated as a single enantiomer (eutomer), since its enantiomeric form can have detrimental effects (distomer).[7,8] Chiral resolution is therefore a cornerstone of most pharmaceutical processes and is currently dominated by chiral column chromatography. In recent years, efforts have been made to find alternatives to column chromatography, and more specifically to the use of its chiral stationary phase. The latter consists of chiral molecules immobilized on micron-sized beads, which are packed inside a cylinder to form a chiral column. A mixture is separated, because one of the enantiomers interacts more strongly with the chiral column. Drawbacks of column chromatograph in general are the relatively high pressures needed to pump through the stationary phase, and a large consumption of solvent. Furthermore, chiral columns are expensive.

Last year, two interesting new methods of chiral separation have been reported, one involving the interaction with achiral perpendicularly magnetized substrates[9], and a second based on a homochiral enantiomer sieving membrane[10], which are not based on mechanical resolution and thus beyond the scope of this tutorial review. Here, we focus on chiral resolution methods from the colloidal to the single molecule level based on mechanical interactions. Some of these methods may one day be contenders to provide an alternative for current resolution methods, and particularly chiral column chromatography.

First, we want to address the scepticism that surrounds mechanical resolution. Chiral resolution using shear flows was initially suggested by Howard et al.[11], but did not have a wide follow-up. Later, Tencer and Bielski put forward predictions that chiral resolution using shear flow will never work at the molecular scale.[12] Indeed, smaller object experience more violent thermal fluctuations, and since chiral lift depends on the orientation of the chiral object (as we will see later), this is problematic. Specifically, rotational diffusion will constantly reorient the chiral object in random directions. Let us introduce the rotational diffusion coefficient D_r for a spherical object of diameter d (eq. 1):

$$D_r = k_B T / (\pi \eta d^3) \quad (1)$$

where k_B is the Boltzmann constant, η the dynamic viscosity of the liquid media, and T the absolute temperature. The Debye relaxation time τ happens to be a good orientation persistence indicator (eq. 2):

[a] Université de Strasbourg, CNRS, ISIS, 8 allée Gaspard Monge, 67000 Strasbourg, France. hermans@unistra.fr
[b] Department of Physics, University of Strathclyde, Glasgow G4 ONG, United Kindom
[c] School of Physics and Astronomy, University of Glasgow, Glasgow G12 8QQ, United Kingdom
[d] Nordita, Royal Institute of Technology and Stockholm University - Roslagstullsbacken 23, SE-106 91 Stockholm, Sweden

$$\tau = 1/(2D_r) \quad (2)$$

A 1 micrometre sized object in aqueous solution at room temperature can thus maintain its orientation for a few seconds whereas a chiral molecule re-orients already after some nanoseconds. Rotational diffusion is thus a serious limitation to chiral migration. The second limitation is due to translational diffusion (i.e., a random walk), also arising from thermal fluctuations that tends to counterbalance changes in concentration built up by mechanical resolution. Considering an approximately spherical object, one can define the competition of chiral drift versus a random walk by numerically deriving the merit number $\beta = y/\bar{y}$. Here, y represents the distance between two enantiomers after a time t drifting away from each other by an angle α (see Fig. 1) and can be derived from the Stokes equation as follows (eq. 3):

$$y \cong F\alpha t/(3\pi\eta d) \quad (3)$$

where F is the drag force, η is the dynamic viscosity of the medium, d the diameter of the spherical object and t time. As mentioned before, chiral migration has to compete with random walk along the y-direction, which according to Einstein and Smoluchowski,[13,14] can be quantified by (eq. 4):

$$\bar{y} = \sqrt{2Dt} \quad (4)$$

with D being the translational diffusion coefficient. Three distinct regimes can be distinguished in Fig. 1c:

- β>>1: Enantiomeric resolution.
- $\beta \simeq 1$: Enantiomeric enrichment.
- β<<1: No resolution.

The smaller the object, the more random walk outcompetes chiral drift, and at the nanometre scale (cf. blue bottom line in Fig. 1), chiral resolution nor enrichment (i.e., not full resolution) can be achieved even after many millennia!

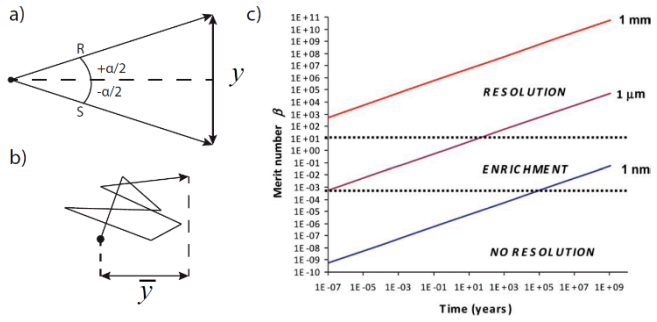

Fig. 1 Competition between chiral drift and random walk. a) Illustration of the distance between 2 enantiomers after an opposite chiral drift by $\alpha/2$ during a time t. Chiral mechanical resolution is limited by the competition with b) random walk resulting from thermal fluctuations. c) Merit number plotted versus time for three sizes (1 mm, 1 µm, and 1 nm) of oriented chiral objects assuming $\Delta\rho$ = 1650 kg/m3 and α = 0.01. Adapted from Ref. 12 with permission from John Wiley & Sons.

This theoretical prediction provided a bleak prospect for actual experimental studies on mechanical chiral resolution. In spite of the latter predications, several experimental studies have revealed promising chiral separations. From these successful experiments it becomes clear that the above picture is too simplistic and that more accurate theoretical descriptions are needed in the future.

2 Crystal sorting

In 1880, the Curie brothers reported what was to be called piezoelectricity. In their work, they were already convinced that this particular effect was dependent on the crystal structure of the material considered. This early discovery aroused the curiosity of Pierre Curie who intensively questioned himself about the role of symmetry on physical phenomena: "*When certain causes produce certain effects, the symmetry elements of the causes must be found in the effects produced. When certain effects reveal a certain asymmetry, this asymmetry must be found in the causes which give birth to them.*"[15] This statement is now known as the "Curie Principle" and caused its inventor to think about the possibility to create an asymmetric environment (useful to perform chiral separation) by juxtaposition of symmetric forces, such as an electric field with a magnetic field. This vision was however vigorously criticized by Barron who suspected it to provide "false chirality".[16] Nevertheless, the possibility to resolve enantiomers without the use of any enantioenriched reagent, material or force was found to be really intriguing and was notably discussed by Welch[17] and De Gennes[18]. The latter hypothesized that a chiral crystal floating on a liquid surface and pushed by a uniform force (such as a jet of air) would experience friction force whose direction directly depends on the shape of the surface in contact with the liquid surface (see Fig. 2).

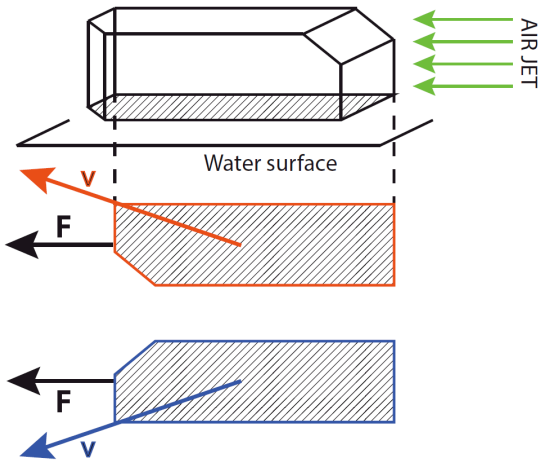

Fig. 2 A Chiral crystal floating on a liquid (the crystal is assumed to be much less dense than the liquid so that its face barely touches the liquid). When having a closer look at its contact area (red, hatched, top view), the velocity v is not parallel to the drifting force F. In fact, we can assume a linear relation between the velocity v and the reaction force: $-R = \bar{\varsigma} v$ with $\bar{\varsigma}$ being a 2x2 symmetric matrix. The anisotropy of $\bar{\varsigma}$ arises from the shape anisotropy of the face in contact with the liquid. If we consider its enantiomer (in blue), the surface anisotropy would yield an opposite motion. If both crystals were dropped at the liquid surface and blown by a uniform air jet, they would travel in opposite direction and thus spatially separate. Adapted from Ref. 18 with permission from Europhysics Letters.

This journal is © The Royal Society of Chemistry 20xx

Please do not adjust margins

In short, enantiomorphic crystals could theoretically experience an opposite tangential motion insofar as their faces in contact with the liquid are mirror images of each other. This suggested method shows that a chiral drift can arise from symmetric forces (here the air jet). For this to be possible, the chiral object must however experience some sort of motion with respect to the fluid just like a boat sailing on the sea that is pushed by the wind and whose motion is constrained by the waterline. In other words, to perform mechanical chiral resolution without the use of an enantioenriched reagent, we can list requirements to fulfill:

1. The top, the bottom, the front and the back of the chiral object must be spatially differentiated (i.e.: orientation persistence).
2. The chiral object must be submitted to some sort of force able to move it along (by external force or passive advection).

Originally puzzled by the fact that Dutch beaches were found to be populated by unequal quantities of left and right shells of bivalves[19], Howard[11] was the first to experimentally explore mechanical chiral separation. In fact, he imagined a way to automate the manual crystal sorting performed by Louis Pasteur[2], with the use of fluid flows. To this end, he used a rotating drum containing millimetre sized chiral crystals immersed in a poor solvent (i.e., to prevent dissolution). The drum rotates about its axis and the rotational speed is chosen to keep the particle well up the side of the drum but not so high that it rotates with the fluid. By doing so, orientation is maintained by gravitational forces produced by near contact of one crystal face with the drum wall and by the finite distance between the centre of gravity of the particle and the centre of hydrodynamic reaction (where torque is applied).

Thanks to this orientation persistence and gravity-assisted motion, Howard[11] could easily resolve enantiomorphic crystals that would move towards opposite ends of the drum (see Fig. 3).

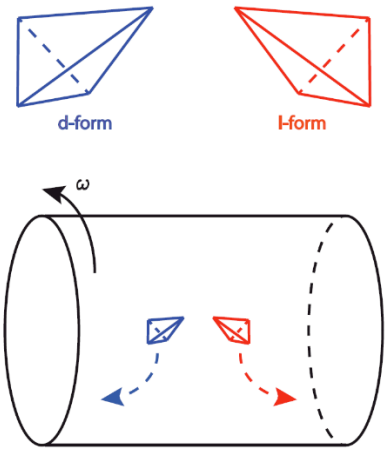

Fig. 3 Method used by Howard[11] to automate Pasteur's manual crystal sorting procedure[2]. It consists of a rotating drum containing millimetre sized chiral crystals immersed a poor solvent. A fine interplay between the centre of mass of the crystal and the reactor force centre facilitates orientation persistence. The weight of the crystal forces it to "fall" along the wall of the drum. Each enantiomer migrates towards a specific end of the drum. Adapted from Ref. 11 with permission from John Wiley & Sons.

This method could easily resolve enantiomorphic crystals even though for some crystals, the top/down spatial differentiation is difficult to maintain. That is, some crystals can have different faces with near equal probability to be facing the wall of the drum. This incomplete orientation can lead to reversal of the migration direction thus preventing enantiomers to be resolved. Similar behaviour was witnessed for large amounts of crystals which can "disturb" each other as well as constantly reorient. The question arises, therefore, whether such a type of mechanical resolution can be scaled down to the molecular level. Welch[17] imagined an elegant new way to achieve the latter. He proposed to use electrophoresis to induce a directional motion of chiral charged amphiphilic molecules trapped at an interface between an organic and aqueous phase (see Fig. 4).

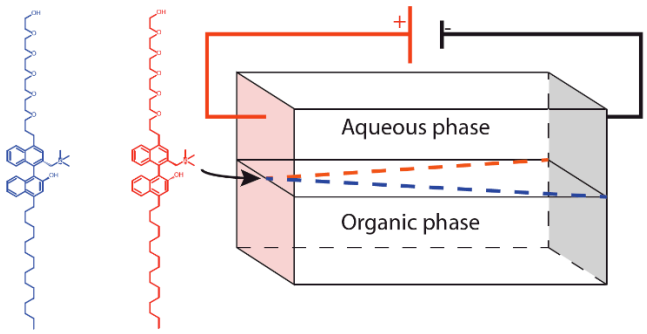

Fig. 4 Electrophoresis device imagined by Welch[17] to separate molecular enantiomers. The chamber is filled with immiscible solvents to form a liquid-liquid interface. An electric field is applied along the chamber. The molecules need to be amphiphilic to be trapped at the interface (top/down spatial differentiation), and charged to be oriented and pulled by one electrode. We show an example of a positively charged Binol amphiphilic derivative that fulfills the above requirements. If introduced through the anode, both molecules should migrate in opposite directions at the interface towards the cathode where they could be collected separately. Adapted from Ref 17 with permission from Taylor & Francis Group.

The electric field was expected to both induce motion of the molecules and to orient the charged part of the molecules towards one electrode leading to a front/back spatial differentiation. Trapping the molecules between the two liquid phases was expected to orient the molecules (whose hydrophilic part would stay in the aqueous phase while its hydrophobic one would remain in the organic phase). The interface would thus allow a top/bottom spatial differentiation. All requirements being fulfilled, the enantiomers should then "sail" in this interface, migrating in opposite directions (in the *xy* plane). Despite its great elegance, this method has yet to be explored experimentally. Moreover, the orientation of the molecule facing towards the anode will be rather inefficient due to thermal fluctuations, and the approach would be applicable only to very specific charged amphiphilic molecules.

3 Resolution in a rheometer

Please do not adjust margins

We previously discussed about different mechanical chiral resolution methods that required the chiral objects to be moved by forces. However, when considering the molecular scale, the list of available methods to actuate the chiral molecules is reduced drastically. Electrophoresis, as discussed above, would only work with charged molecules. Similarly, magnetophoresis would require strongly paramagnetic species and very high magnetic field gradients.

It is not strictly necessary to exert a direct force on the chiral object (thus achieving driven transport). One can also rely on (passive transport using) fluid flows to produce chiral specific drifts provided that symmetry is broken beforehand.

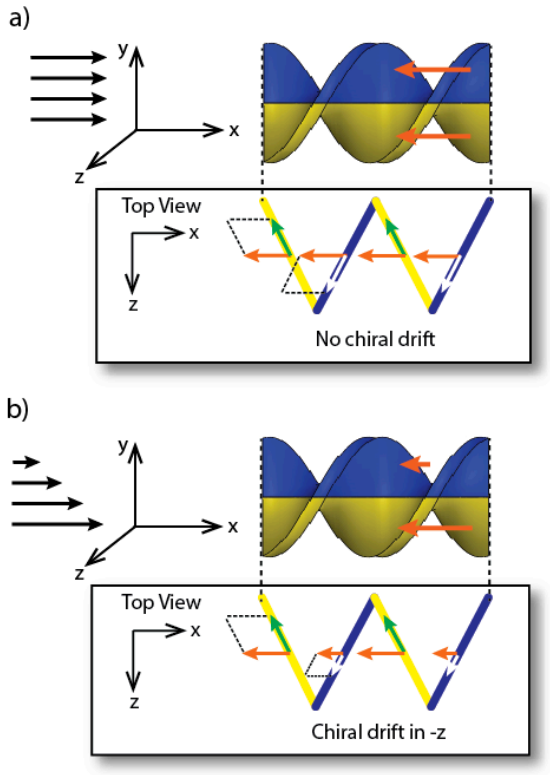

Fig. 5 A qualitative understanding of chiral lift on a twisted ribbon. Blue and yellow shading indicate the top and bottom halves of the ribbon. The drag force acting on the top part of the ribbon (cf. orange arrow) has a component along +z whereas the drag force acting on the bottom part of the ribbon is along the –z direction. a) In a symmetric flow profile, both sides are experiencing equally large opposing forces, which cancel each other out. b) In an asymmetric flow, the net drag force acting on the ribbon is ≠ 0 and chiral drift is possible (note: compare the lengths of the green vs. white arrows).

Let us consider a right-handed twisted ribbon. This ribbon can be separated in two halves along its longitudinal axis (cf. Fig. 5 in blue and yellow). We assume for simplicity that the chiral object is aligned in the flow direction. When the ribbon moves through the fluid, it experiences a drag force opposite to the direction of the oncoming flow (where the velocity is proportional to the black arrows in Fig 5, while drag force is represented by orange arrows). The interaction of the fluid with the blue side of the helix will generate a drag force with a component along the +z direction (white arrow), while the interaction with the yellow halve generates a drag force in the –z direction (green arrow). In a uniform velocity profile, both sides of the helix experience the exact opposite lift forces: no chiral drift would be observed (Fig 5a). However, if the flow profile is asymmetric (see Fig. 5b), the forces on one halve will outcompete the other half (here yellow surpasses blue) and an overall chiral drift will emerge.

In other words, it is not necessary to move an oriented chiral object in fluids to create a chiral-specific lift: shear flows can carry the particles along instead. Using shear flows allows the experimentalist to focus only on the orientation persistence of the chiral object and no longer on the ways to move it along.

3.1 Taylor-Couette flow

In 1890, Maurice Couette publicly presented a new concentric viscometer, which he had used to accurately measure the viscosity of fluids and later on to study boundary conditions to make sure that the "no-slip" condition was verified for a range of materials and fluids.[20] He had no idea at that time that more than a century later his rheometer would have had another virtue: the capability to discriminate between enantiomers. Let us consider a Couette cell made of two concentric cylinders with R_o being the outer radius of the inner one and R_i the inner radius of the outer one. The outer cylinder turns with an angular velocity Ω. The shear rate at a radial position r can be defined as (eq. 5):

$$\dot{\gamma} = 2\Omega / (r^2(1/R_o^{\,2} - 1/R_i^2)) \quad (5)$$

The anisotropy of the flow generated in the annular gap allows discrimination between enantiomers (as explained in Fig. 5). In other words, if the outer cylinder is rotated clockwise (CW), a left- handed helix (blue) will experience a chiral lift in the vorticity direction and will migrate to the top of the cell. A right-handed helix (red) will experience an opposite force and will thus migrate towards the bottom. If the rotation direction is reversed, the migration directions are also reversed (see Fig. 6).

In a compelling numerical simulation, following Kim's initial work[21], Makino and Doi[22] studied the migration of twisted ribbons in (circular) Couette flow. They showed that enantiomers move in opposite directions with a velocity $\langle v_z \rangle$ expressed by eq. 6:

$$\langle v_z \rangle = \lim_{t\to\infty}(Z(t))/t \quad (6)$$

where *Z(t)* is the average *z*–coordinate of the 1000 particles considered in their simulation. They were able to verify how far this mechanical chiral lift force could be scaled down in terms of particle size. In particular, they defined two regimes depending on the particle size (eq. 7 and eq. 8):

$$\langle v_z \rangle \propto \gamma a \text{ when } Pe = \gamma / D_r \geq 1 \quad (7)$$

and

$$\langle v_z \rangle = \gamma a(\gamma / D_r)^2 \text{ when } Pe = \gamma / D_r \leq 1 \quad (8)$$

This journal is © The Royal Society of Chemistry 20xx

Please do not adjust margins

with a being the width of the twisted ribbon and D_r the rotational diffusion coefficient. For a given shear rate, decreasing the size of the chiral object will thus increase its rotational diffusion resulting in the loss of the chiral lift force it experiences. To counter this effect and recover a decent chiral lift, one can either increase the shear rate (by increasing the radius of the cylinders, decreasing the gap, or increasing the rotation speed) or try to decrease the rotational diffusion of the chiral objects by aligning them with an electric field for example. According to their numerical simulation, a set of concentric cylinders with a 10 cm radius, and a gap distance of 1 mm rotating at 100 rpm could be enough to cause migration of a 10 nm chiral object over 1 mm in a few minutes.

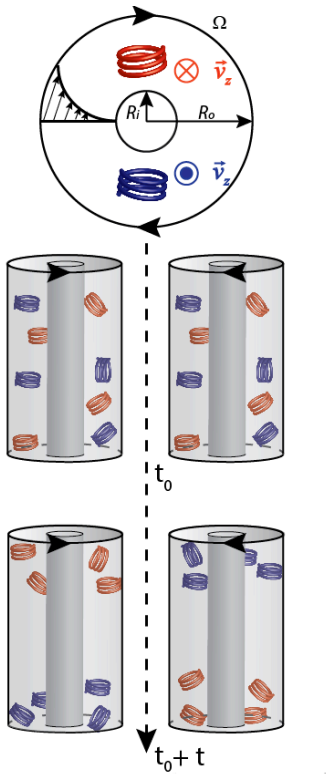

Fig. 6 Chiral drift experienced by two enantiomeric structures in a Taylor-Couette cell. At time t_0 a racemic mixture is placed in the cell. After a certain time t full chiral resolution is achieved depending on the shear rate and the size of the helices.

Hermans et al.[23] implemented an experimental model system to separate enantiomers using a circular Couette flow. Hermans found that by confining 2D chiral objects at the air-liquid interface in the Couette gap, an in-plane chiral force could be induced (i.e., in the radial direction).[23] This approach allowed them to provide not only an average drifting motion but also a detailed rotational and translational motion in time, which could in turn be compared to the hydrodynamic model they developed. SU8 photoresist chiral objects were fabricated and placed at the surface of silicon oil in between the two cylinders. The particles revolved around the cell with a constant velocity v_θ but experienced large variations in their angular velocity ω known as the so-called Jeffery orbit for elongated particles. The circular Couette flow induced a chiral specific radial drift as shown in Fig. 7.

The directionality and amplitude of the observed effect, according to their numerical considerations, are expected to be related to the shape of the chiral object, the largest drift velocities being expected for asymmetric particles with a high aspect ratio. A series of stochastic simulations allowed them to assess the possibility to discriminate between smaller enantiomers (micro- or nanometre scaled chiral objects). Interestingly, the in-plane chiral drift scales linearly with time, whereas diffusion scales with the square root of time. The latter suggests that over long times, chiral drift could outcompete diffusion at the molecular scale. A three-dimensional version of these experiments is currently being studied by Hermans and co-workers.

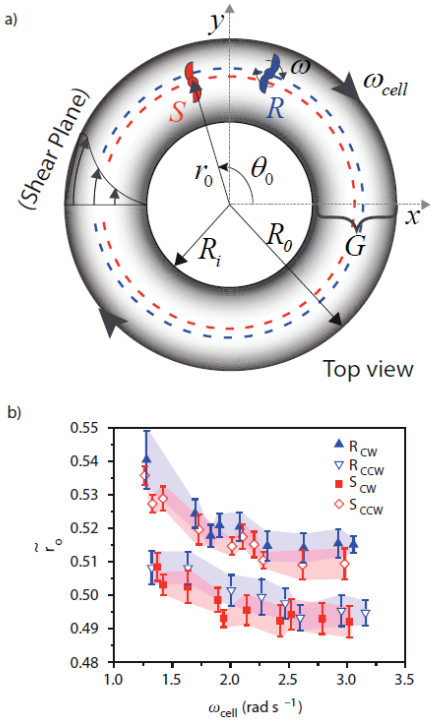

Fig. 7 Chiral resolution at the air/liquid interface using a Taylor-Couette cell. a) Top view of the Couette-cell used, consisting of two concentric cylinders. The outer cylinder has a radius R_o while the inner one has a radius R_i. The gap $G = R_o - R_i$ is filled with oil. Right- (blue) and left-handed (red) chiral objects are floating at the air-liquid interface. Once the outer cylinder starts turning with an angular velocity ω_{cell}, b) one can see a chiral specific drift in the radial position ($\tilde{r_0} = (r_0\text{-}R_i)/G$) of the enantiomer R or S, which also depends on the turning direction, clockwise (CW) or counter-clockwise (CCW). Adapted from Ref. 23 with permission from Springer Nature.

3.2 Rotating parallel discs

A different type of rheometer consists of two parallel discs, spaced by a distance h (see Fig. 8). The upper disc rotates whereas the lower one is fixed. Makino and Doi[24] showed both experimentally and numerically that shear flow in such a parallel-plate rheometer (see Fig. 8) could resolve enantiomers at the millimetre scale. Specifically, they fabricated chiral cubes by cutting two edges to produce D- and

Please do not adjust margins

L-particles. The two cuboid enantiomers exhibited a net opposite drift in the vorticity direction. One enantiomer will experience a drift towards the centre of the disc whereas the other will migrate towards the outer radial region (see Fig. 8 c). For the opposite rotation direction, for symmetry reasons, the migration directions of each chiral object also reversed. As mentioned before,[22] the migration velocity $\langle v_z \rangle$ depends on the Peclet number (*Pe*) and is given as (eq. 9 and eq. 10):

$$\langle v_z \rangle = Ba\gamma Pe^2 \text{ when } Pe = \gamma / D_r \leq 1 \quad (9)$$

and

$$\langle v_z \rangle = Ca\gamma \text{ when } Pe = \gamma / D_r \geq 1 \quad (10)$$

where *B* and *C* are chirality index constants (if the object is not chiral, *B* and *C* are equal to zero and there is no drift), *a* is the particle size and $\dot{\gamma}$ is the shear rate.

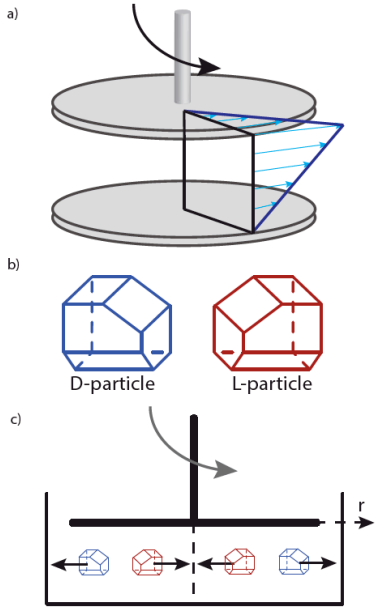

Fig. 8 Rotating parallel discs setup[24]. a) Both discs are parallel. The upper one can turn while the lower one cannot. The velocity profile generated is depicted in blue. b) D- and L-particles sculpted in silicon rubber. c) Once the D- and L-particles are immersed in an almost density matched silicon oil in the gap and when the upper disc is rotating CCW (in this particular case), both enantiomers migrate oppositely in the vorticity direction (along the r axis). Adapted from Ref. 24 with permission from the Physical Society of Japan.

Once again, one can notice that Makino and Doi[24] were concerned about the possibility to downscale this effect down to the molecular level. In their model, the drift velocity does not scale linearly with the shear rate, which forces one to drastically increase the shear rate to be able to resolve molecular enantiomers. Their experimental results were numerically verified and they could correctly predict the direction of migration of the chiral objects, but interestingly the observed drift velocity is much higher than predicted (by two orders of magnitude). They attributed this discrepancy to the effect of the wall that could better align the particle, and thus enhance the effect of the flow.

4 The propeller effect

In 1978, Baranova and Zel'dovich[25] predicted that the "propeller effect" could be used to separate enantiomers in a racemic mixture. More specifically, the use of a radio-frequency electric field of rotating polarization can couple to the electric dipole moment of a molecule inducing its rotation. A subsequent rotational-to-translational coupling then allows enantiomers to migrate in opposite directions (due to their inherent opposite right-left asymmetry). This effect was expected to survive the randomization of Brownian motion and yet, no experimental evidence was provided until recently.

4.1 At the colloidal scale

In 2013, Fisher and co-workers[26] performed a proof concept at the colloidal scale (Fig. 9). The latter was considered as an ideal scale to study the propeller effect where the nano-structures used could be seen as "colloidal molecules" in mesoscopic systems. In this way, it was possible to directly visualize the phenomenon, which would be very challenging at the molecular scale. In their study, they replaced the electric dipolar molecule and the rotating electric field with a magnetic field acting on a magnetic dipolar colloid. The colloidal structures used were grown via Glancing Angle Deposition (GLAD), which allowed the production of large quantities of helices of defined size and shape. The colloidal helices are magnetized orthogonally to their long axis. By doing so, they acquire a magnetic moment that allows a magnetic field to apply a torque τ_{mag} on the helix (eq. 11):

$$\tau_{mag} = m \times B \quad (11)$$

Where *m* is the magnetization of a colloidal helix and *B* the magnetic field. The micrometre objects are also subjected to a viscous drag τ_{drag} (eq.12):

$$\tau_{drag} = XR^3 \eta \Omega \quad (12)$$

where *R* is the colloid's characteristic size, *X* is a scale-free geometry factor that depends on the shape, η is the fluid viscosity, and Ω is its speed of rotation. At low magnetic field rotation velocities, the moment of the particle will align with the field and maintain a constant velocity $\Omega = \omega$ with the two torques balancing each other. The subsequent rotational-to-translational coupling allows the structures to move in solution. For symmetry reasons, two enantiomers will migrate in opposite direction with a velocity υ (eq. 13):

$$\upsilon = \varepsilon \Omega \quad (13)$$

where ε is the rotational-to-translational coupling constant, which directly depends on the pitch of the helix thus suggesting that the "degree of chirality" dictates the propulsion efficiency.
The authors compared the strength of the dipole coupling with thermal fluctuations (eq. 14):

$$S_{mag} = mB / k_B T \quad (14)$$

This journal is © The Royal Society of Chemistry 20xx

Please do not adjust margins

S_{mag} is of the order of 10^3, which means that in their experiments the dipole coupling is much larger than thermal fluctuations, thus explaining the separation observed. However, if we go back to Baranova's idea (electric field driven molecules)[25], the structures are much smaller, and the propulsion efficiency is on the order of 10^{-4}. Based on the latter observations, resolution of enantiomers at the molecular scale seems hopeless.

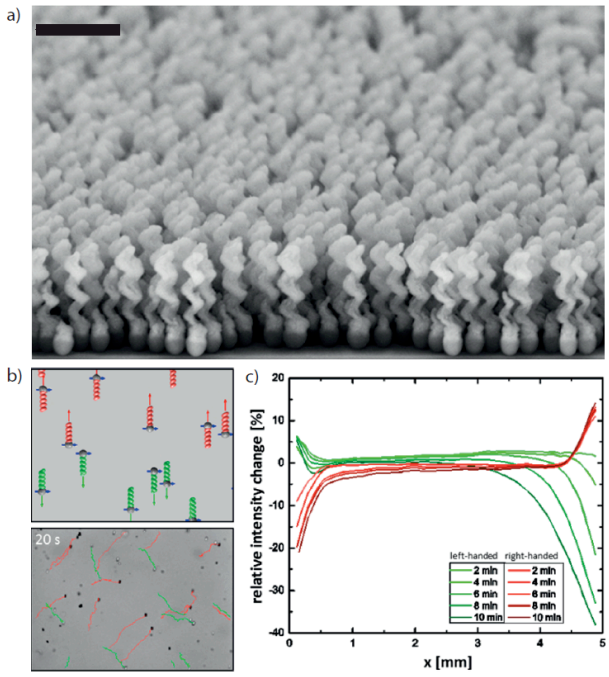

Fig. 9 The propeller effect at the colloidal scale. a) SEM images of a wafer containing helices representative of those used in Ref. 26 obtained through glancing angle deposition. Scale bar is 2 μm. b) When a field is applied, the magnetic moments of the helices (perpendicular to their long axis) aligns with the field direction and rotates with it. The rotational-to-translational coupling then allows right- and left-handed helices to move in opposite directions. c) Relative intensity change with time of the scattering intensity across the width of a 5 mm cuvette filled with a suspension of right- or left-handed colloids in a rotating magnetic field of a strength of 50 Gauss and a frequency of 40 Hz. Adapted from Ref. 26 with permission from the American Chemical Society.

4.2 At the molecular scale

Clemens and coworkers[27] nevertheless did attempt to perform chiral separation at the molecular scale. To this end, they surrounded a capillary tubing with four electrodes (see Fig. 10) alternatively switching between "high field" (1100 V) and "zero field" values allowing a proper rotation of the electric field in four phases. Each phase corresponds to a 90° turn, and was able to orient a chiral binaphthyl molecule.

As explained, enantiomers were expected to move in opposite directions with a translational velocity u resulting from the rotational-to-translational coupling and expressed by (eq. 15):

$$u = L_{ref} u_{eff}(E) A_{corr}(E) F(E) \qquad (15)$$

where $u_{eff}(E)$ is the effective molecular rotation frequency, L_{ref} is the value of one displacement per one revolution and $A_{corr}(E)$ is the angular correction factor and accounts for the random orientation of the molecular propeller's axis. $F(E)$ corresponds to the "responding" fraction of molecules that follow the changes in electric field direction resulting in directional propeller motion. In fact, a large fraction of molecules rotates equally in both directions and therefore they do not contribute to propeller propulsion.

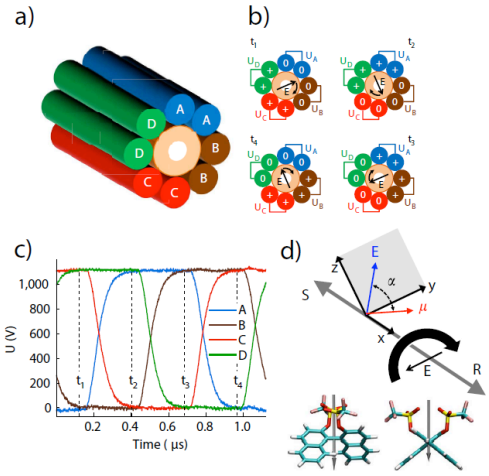

Fig. 10 Rotating electric field-assisted propeller effect. a) Cartoon representing the separation capillary chamber surrounded by four electrodes (A, B, C and D). b) Cross-sectional cartoons showing how the electric field rotates. One can decompose a 360° complete rotation in four phases characterized by four consecutive time points (t_1, t_2, t_3 and t_4). c) Voltage of the four electrodes as a function of time during one cycle. d) Predicted direction of migration of R- and S- forms of 1,1'-Bi-2-naphthol bis(trifluoromethanesulfonate) when submitted to a clockwise rotating electric field. The field rotates about the x-axis in the yz plane and forms an angle α with the dipole moment of the molecule. The structure of the S molecule is also shown to highlight its propeller shape that optimizes the resulting lift (grey arrows) inherent to the rotation of the molecule in the fluid. Adapted from Ref. 27 with permission from the Royal Society of Chemistry.

The responding fraction of molecules $F(E)$ can then be expressed as the ratio of molecules following the rotation of the electric field over the total number of molecules (eq. 16):

$$F(E) = 1 - \frac{2\mu E}{k_B T(e^{2\mu E/K_B T} - 1)} \approx \frac{2\mu E}{k_B T} \qquad (16)$$

where μ and E are the absolute values of the dipole moment and electric field magnitude. T is the temperature and k_B the Boltzmann constant. Assuming an electric field magnitude of 6 × 10^5 V m^{-1} and a molecular electric dipole moment of 5.3 Debye, they estimated the number of molecules rotating with the electric field to be only 5 molecules out of 1000. To verify their theoretical expectations, the capillary chamber was filled with a solution of 1,1'-Bi-2-naphthol-bis(trifluoromethanesulfonate), which was submitted to a rotating electric field (REF) for 83 hours and subsequently eluted out of the microfluidic channel. The eluted fractions were analysed by circular dichroism (CD) and UV-vis spectroscopy (Fig. 11) showing enrichment along the capillary, which is consistent with the propeller theory arguing that the two enantiomers move in opposite directions.

Please do not adjust margins

Furthermore, when the REF is switched from CW to CCW, both enantiomers reversed their migration direction. This study convincingly shows that chiral drift *can* compete with Brownian motion at the molecular level.

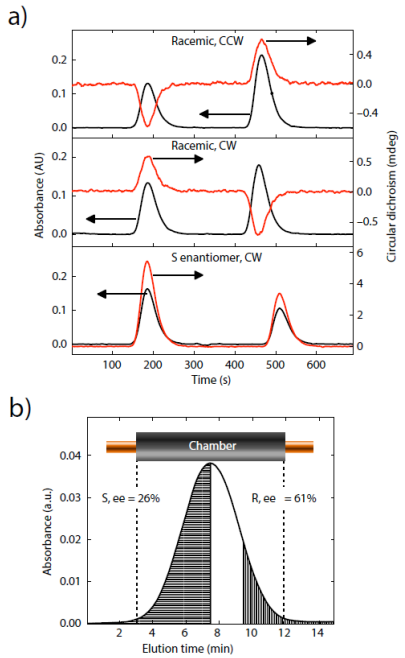

Fig. 11 Enantioenrichment of a racemic mixture of the 1,1'-Bi-2-naphthol bis(trifluoromethanesulfonate) molecules after 83 hours of REF. a) (Top) Absorbance and Circular Dichroic chromatograms of a racemic mixture while turning the field CCW (middle) CW and (bottom) CW for the pure S enantiomer. One can see on the chromatograms that the leading and the trailing fractions of the chamber display opposite CD signals that is reversed when the rotation direction of the field is reversed. (Bottom) When a pure S enantiomer is loaded in the cell and submitted to the same experimental condition, both fractions display a CD signal of the same sign which is a control experiment for chiral migration observed in the previous racemic experiments. b) Absorption chromatogram of the chambers slug after being exposed a CW REF collected from the in-line detector. The slug can be decomposed in two halves (grey areas). The first left halve was enriched with the (S)-1,1'-Bi-2-naphthol bis (trifluoromethanesulfonate) whereas the second one was enriched with the R-analogue by 61 percent. Adapted from Ref. 27 with permission from the Royal Society of Chemistry.

5 Resolution in microfluidic devices

Microfluidic devices are microchip-based integrated fluidic circuits that can perform one or several (bio-)chemical laboratory functions on a sub-millimetre scale. They offer numerous capabilities that are of great use in practice, like easy fabrication, high portability, the processing of tiny amounts of samples and reagents, high processing speeds and short reaction times, parallel operation, low costs etc.[28] Ultimately, many advances in the field of microfluidic devices are inspired by the vision of integrating an entire biochemical laboratory onto a single microchip ("lab-on-a-chip"). For these reasons, the miniaturization of classical, chemistry-based enantioseparation techniques to the microchip format is a rapidly advancing area of research[29,30] since its first realization around 25 years ago[29]. Concerning chiral separation by mechanical means, it turns out that microfluidic devices provide an ideal environment for theoretical developments and experimental proof-of-concept studies.

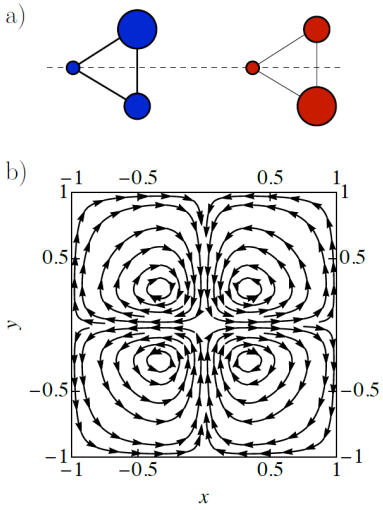

Fig. 12 a) Illustration of the two-dimensional model for chiral particles proposed by Kostur et al.[31] Spherical component "atoms" or chemical "groups" (symbolized by the coloured circles) of different size are rigidly connected (solid lines) to form a rigid particle or "molecule". Due the different sizes of the individual "atoms", such a two-dimensional particle has a specific handedness. The two enantiomers of triangular shape particle are shown in blue and red; the dashed line indicates the mirror symmetry axis. b) 4-vortex flow pattern in the two-dimensional x-y plane, employed by Kostur et al.[31] (and later by Burger and Beleke[32,33]) to study chiral separation in micro-flows. Streamlines of the fluid flow $(v_x, v_y) = (\partial\psi / \partial y, \partial\psi / \partial x)$ obtained from the stream function $\psi(x, y) = \sin(\pi x / L_x)\sin(\pi y / L_y) / [2 - \cos(\pi x / L_x))(3 - 2\cos(\pi y / L_y)]$ with $L_x = L_y = 1$ are shown. Adapted from Ref. 31 with permission from the American Physical Society

5.1 Vortex flows

The first proposal to use micro-flows for mechanical chiral separation appeared in 2006 with a theoretical study by Kostur et al.[31] They considered an open microfluidic setup on a planar piezoelectric substrate, in which fluid flow is agitated within a thin liquid layer on the substrate by surface acoustic waves. This setup had been motivated by an earlier experimental demonstration[34] that surface acoustic waves, which correspond to a quadrupolar force density, create a flow pattern of four, pairwise counter-rotating vortices arranged on a rectangular lattice, see Fig. 12b. Kostur et al. used a simplified 2-dimensional model of this 4-vortex streaming pattern to investigate its effect on 2-dimensional chiral particles. The chiral particles were constructed from three rigidly connected "atoms" with different friction coefficients arranged in a triangular pattern; see Fig. 12a. Two enantiomers of opposite handedness are related to each other by switching two out of the three "atoms'' in the triangular sequence (it is easy to see that this operation is equivalent to mirroring the particle in the 2-dimensional plane). Each "atom" experiences a hydrodynamic friction force, which is proportional to its velocity relative to the fluid with a proportionality constant equal to the "atom's" friction coefficient. These particles

This journal is © The Royal Society of Chemistry 20xx

Please do not adjust margins

therefore feel a mechanical force in a fluid flow, which is sensitive to their chirality. Moreover, it is straightforward to take into account diffusive motion by adding thermal fluctuating forces in the equation of motion.

By extensive numerical studies, Kostur et al.[31] demonstrated that the purely advective motion (without thermal fluctuations) within each one of the vortices from Fig.12b is governed by a set of deterministic attractors, which is characteristic for the particle's chirality and the flow orientation in the vortex. Under the influence of weak thermal noise, almost all enantiomers of a specific chirality consequently settle in that attractor that has the highest stability for the given chirality. Hence, after reaching the stationary state, the two different types of fluid vortices (with left-handed or right-handed flow orientation, see Fig. 12b) contain different amounts of a specific enantiomer. In other words, Kostur et al.[31] predicted from their model that an enantiomeric mixture can be separated mechanically by using fluid vortices in a microfluidic device as "chiral selectors''.

The model of Kostur et al.[31] is based on a few quite drastic simplifications. Most importantly, it is restricted to two dimensions, the chiral particles do not act back on the hydrodynamic flow field such that hydrodynamic interactions between the component "atoms" are neglected, and the bonds between these "atoms'" are rigid, prohibiting particle deformations. Despite these simplifying assumptions, Kostur et al.[31] argue that their model does capture the relevant aspects of symmetry and thermal noise in the motion of chiral objects. As for the first simplification, one could think about confining the chiral objects to a surface or a liquid-liquid interface[17] in a way that also suppresses out-of-plane rotations, such that effectively the system is two-dimensional (see Fig. 4 above).

Concerning hydrodynamic interactions, two follow-up studies[32,33] analysed the same 4-vortex flow pattern and its potential for chiral separation employing two different computational methods, which both allow for a full hydrodynamic treatment of the problem. The first study[32] uses a so-called fictitious domain Lagrange multiplier method, which has been developed specifically to capture the deterministic motion of rigid particles in carrier fluids. The second study[33] uses a finite element immersed boundary method. Both techniques numerically solve the two-dimensional incompressible Navier-Stokes equations for the fluid velocity field in the presence of the immersed particles together with their rigid body equations of motion. The validity of this model and the numerical methods have been verified by comparing experimental trajectories with trajectories obtained from the numerical simulations for both, non-chiral and chiral particles. Left-handed and right-handed L-shaped enantiomers were used as chiral particles, with their long "leg" being about 300 μm and their short "leg" about 200 μm in length. For such relatively large particles, the effects of thermal fluctuations are negligibly small. Both studies[32,33] consistently predicted that these enantiomers are separated in the 4-vortex flow according to their handedness when injected into the flow approximately in the middle between two counter-rotating vortices, because left-handed (right-handed) enantiomers are attracted by clockwise rotating (counter-clockwise rotating) vortices to circle around their centres.

While in the finite element immersed boundary method[33] the particles are perfectly rigid, the fictitious domain Lagrange multiplier method[32] allows to even consider deformable particles. Indeed, the simulations were performed for slightly deformable L-shaped enantiomers, but did not show qualitative differences to the rigid particle simulations in Beleke-Maxwell et al.'s work.[33]

Two earlier studies[35,36] had investigated flexible chiral particles, which are built of "atoms" connected by elastic springs, when moving in three-dimensional uniform shear flows. For helical particles, Talkner et al.[36] showed from numerical simulations that hydrodynamic interactions between the component "atoms" (via the Rotne-Prager mobility tensors) lead to mechanically induced drift in a direction lateral to the shear plane, which depends on the chirality of the object and the sign of the shear rate. It even turned out that the shear flow can deform achiral flexible particles into chiral shapes, which then experience a similar lateral drift motion. Such shear-induced chirality and lateral migration had been reported by Watari and Larson[35] for symmetrically shaped tetrahedral objects with anisotropic rigidity. In both studies[35,36] thermal noise effects had been neglected.

From the practical viewpoint of integrating microfluidic chiral separation concepts into "lab-on-a-chip'" systems, easy access to the purified enantiomers for further processing or extraction is essential. In the Kostur et al.[31] proposal, particles with specific chirality are spatially accumulated within defined regions of the 4-vortex flow. A convenient alternative may be to make the two chiral partners move with different average velocities along a linear channel by imposing suitable flow patterns. In this way, a first "plug" enriched in one enantiomer arrives at the end of the channel before a second "plug" containing the other enantiomer, much like in the microchip electrophoretic versions of conventional separation techniques[29,30]. Mechanical chiral resolution concepts in linear microfluidic channels have been studied up to date in several contributions, both theoretically[37–39] and experimentally[40,41].

5.2 Microfluidic channels

In a straight channel with a regular cross-sectional shape, pressure-driven flows develop a typical parabolic velocity profile[42]. In particular, in a channel with a rectangular cross-section and a high aspect-ratio (width/height), the flow profile is parabolic in the height direction and uniform over the whole channel width. The corresponding shear rate varies linearly over the channel height with negative (positive) sign in the upper (lower) half of the channel. Marcos et al.[40] studied the motion of helically shaped bacteria of about 16 μm in length in such a parabolic Poiseuille flow. They observed a lateral drift motion perpendicular to the flow with a direction that depends on the chirality of the helix and the sign of the shear rate, i.e. an effect similar to the one observed in rheometers

Please do not adjust margins

(see Sec. 3) and to the one predicted for flexible particles by the numerical studies of Watari and Larson[35], and Talkner et al.[36] For symmetry reasons the lateral drift in the Poiseuille profile was oriented in opposite directions in the upper and lower half of the channel. The analysis of Marcos et al.[40] revealed that for the lateral drift to occur preferential alignment of the helical bacteria with the streamlines of the flow is required. If rotational Brownian motion due to thermal noise dominates over the alignment effects due to the flow, the bacteria are randomly oriented and the latter drift disappears. Marcos et al.[40] estimated that with currently available microfluidics technology, shear rates of the order of 10^7 s^{-1} can be generated, sufficient to induce lateral drift motion of helical particles as small as 40 nm.

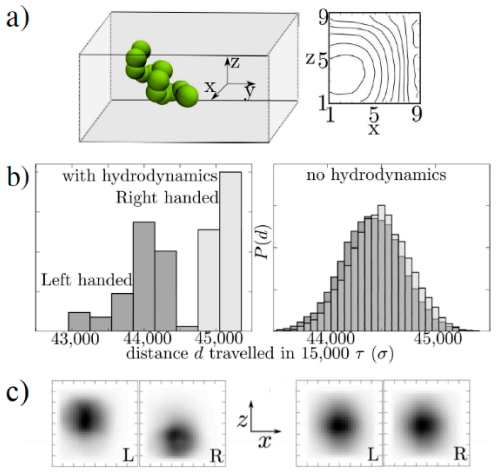

Fig. 13 a) Illustration of the set-up simulated by Meinhardt[39] using dissipative particle dynamics. The chiral helical particle (green object) is advected along the y-direction through a microchannel (grey rectangular box) with square cross-section (x-z plane) by a pressure-driven fluid flow, which is asymmetric due to different hydrodynamic boundary conditions on the four channel walls. The right panel shows profiles of equal flow velocities across the channel. b) Separation of right-handed and left-handed helical particles. Histograms of distances travelled along the channel axis (y-direction) in a certain time for left-handed helices (dark shaded) and right-handed helices (light shaded) are shown. Results from simulations, which take full account of hydrodynamic effects (left part), are compared to a simple Brownian dynamics simulation without hydrodynamics (right part). c) Distributions for left-handed (L) and right-handed (R) helices across the channel in the two cases with and without hydrodynamics. The quantities σ and τ represent the basic length and time-units in the simulation model. Adapted from Ref. 39 with permission from the American Physical Society.

Since the upper and lower halves of the Poiseuille profile in the channel induce drift motions in opposite directions, a racemic mixture would separate into four quadrants in the plane perpendicular to the flow, with diametrically opposed quadrants containing the same enantiomer. However, both enantiomers would still move with identical (average) velocities along the channel. The prospects of distinguishing the two enantiomers by distinct migration velocities along a microfluidic channel have further been investigated in Reference [37–39,41].

The first two studies[37,38] are based on the simple two-dimensional rigid particle model introduced by Kostur et al.[31] By analyzing the advective and diffusive motion of such chiral particles in two-dimensional linear channels in the low Reynolds number regime, Eichhorn[37,38] showed that particles with opposite chirality move with different average velocities if the flow patterns break mirror symmetry. Specifically, Eichhorn[37,38] considered two possibilities for nonlinear flows with broken symmetry: first, a pressure-driven parabolic flow profile in a two dimensional straight channel superimposed with a linear electroosmotic shear flow, which is created by different slip velocities at the two channel walls[42] ; second, a pressure-driven flow through a two-dimensional channel with a straight and a periodically structured channel wall, leading to a periodic nonlinear flow pattern with broken mirror symmetry. The theoretical analysis,[37,38] showed that the two enantiomers, while being advected by the fluid flow, rotate in slightly different manners with different preferential orientations. Moreover, the momentary advection speed of an enantiomer results from the combined effect of the local fluid flow acting on all the component “atoms'”, and therefore depends on the particle's angular orientation. The net effect is an average transport velocity through the channel, which is characteristic for the specific chirality of the particle.

The model used by Eichhorn[37,38] is based on simplifications similar to Kostur et al.[31]: the hydrodynamic interaction between the component “atoms” of a rigid chiral particle are neglected (see Fig. 12), and the analysis is restricted to two dimensions. That chiral separation indeed can be observed in a fluid flow without hydrodynamic interactions implies that the separation process is not a direct consequence of the hydrodynamic nature of the forces acting on the component “atoms”. Hence, it would occur under any suitable driving force, whose effect on these “atoms'” results in an overall chirality, such as an electric field applied on chiral particles which consist of “atoms” or “chemical groups” with different charges[38]. The two-dimensional setting, however, is quite unrealistic as a description of real microfluidic channels. Nevertheless, the analysis of the 2-D model provides important insights[37,38] in accordance with the conclusion of Kostur et al.[31]: as long as thermal noise does not dominate over deterministic forces, mechanical chiral resolution occurs in force fields that break chiral symmetry (and thus have specific parity or “chirality” themselves) by spatial variations of force direction and magnitude on scales comparable to the size of the chiral objects. Guided by these insights, Meinhardt et al.[39] proposed a method for chiral sorting in a straight microfluidic channel with quadratic cross-section. In order to create the required asymmetric flow profile from a pressure difference applied to the channel ends, they suggested that the channel walls be endowed with different hydrodynamic boundary conditions (e.g. slip lengths) by chemical functionalization[43]. Meinhardt et al.[39] studied the migration of helical chiral particles in the channel (see Fig. 13) by dissipative particle dynamics simulations[44], a mesoscale computational method which takes full account of hydrodynamic interactions. They demonstrated that helices of opposite chirality move with different average speeds and thus can be separated. By contrasting simulations with and without hydrodynamic interactions, Meinhardt et al.[39] could show that the separation effect without hydrodynamic interactions, as predicted by

This journal is © The Royal Society of Chemistry 20xx

Please do not adjust margins

Eichhorn[37,38], is very weak, and that effective separation is actually driven by hydrodynamics (see Fig. 13).

An actual experimental separation of colloidal chiral particles in a rectangular microfluidic channel has been performed by Aristov et al[41]. Rather than breaking chiral symmetry of the flow profile by asymmetric coatings of the channel walls, they made use of a topographical structure consisting of periodically arranged ridges (see Fig. 14), which was known to create a helical flow field[45] with a circulation direction fixed by the orientation of the ridges relative to the pressure drop over the channel.

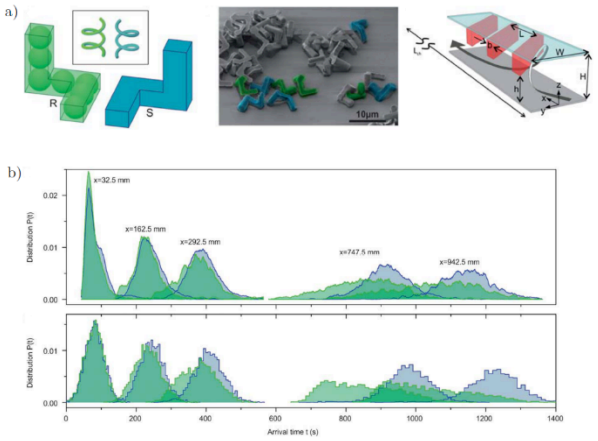

Fig. 14 a) Experimental set-up used by Aristov et al.[41] The left panel shows the schematic illustration of particles of opposite chirality R (green) and S (blue). They consist of three mutually perpendicular "legs" of equal length (about 6 μm) as simplified representations of real helices. In the theoretical model, the chiral colloids have been represented by 7 rigidly connected beads. The middle panel shows an false-coloured SEM micrograph. The right panel shows a schematic of the microfluidic channel (side walls not shown) with periodically arranged oblique ridges (red) which create a swirling flow pattern (W=150 μm, H=115 μm, H-h=50 μm, b=40 μm, L=146 μm, and L_{ch}= 1 m). (b) Arrival time distributions at various fixed positions x along the channel axis from experiments (upper panel) and simulations (lower panel) demonstrating separation of the chiral colloidal particles in a right-handed helical flow field. Adapted from Ref. 41 with permission from the Royal Society of Chemistry.

Chiral colloidal "test" particles of several micrometer in size were fabricated from photoresist SU-8 (see Fig. 14). In the separation experiment, a racemic mixture of left-handed and right-handed such particles was injected into the channel and then driven to move along the channel by a swirling flow field with right-handed circulation direction. Aristov et al.[41] measured the concentration of each enantiomer at different positions along the channel and found that the right-handed particle species with a chirality that matches the chirality of the flow pattern was transported with higher velocity than the left-handed particles (see Fig. 14). Numerical simulations of the experimental set-up, based on a Brownian dynamics model including hydrodynamic interactions via a grand mobility tensor[41], showed excellent agreement with the experimental observations. Detailed analysis of the experimental data and the numerical data revealed that the right-handed particle were accumulated in the channel centre, where flow velocity is high, while the left-handed particles preferably visited regions with low flow velocities closer to the channel walls. Aristov et al.[41] estimated that current microfluidics technology should allow to separate particles of about 120 nm in size in a channel with about 3.2 μm cross-sectional dimension and 3 cm length.

6 Resolution in non-chiral microlattices

A quite different route towards chiral separation in microfluidic devices was explored by the theoretical study[46] and the experimental follow-up[47]. Rather than built-in structural chirality in the flow pattern or channel shape, they exploited dynamical chiral symmetry breaking in non-chiral lattice potentials[46] or post arrays[47]. Conceptually, this approach builds on the observation of de Gennes[18] (see Section 2) that small chiral objects, when sliding down an inclined plane or floating over a liquid surface (see Fig. 2), should generically move in directions slightly different for the two enantiomers, provided that thermal noise is negligible.

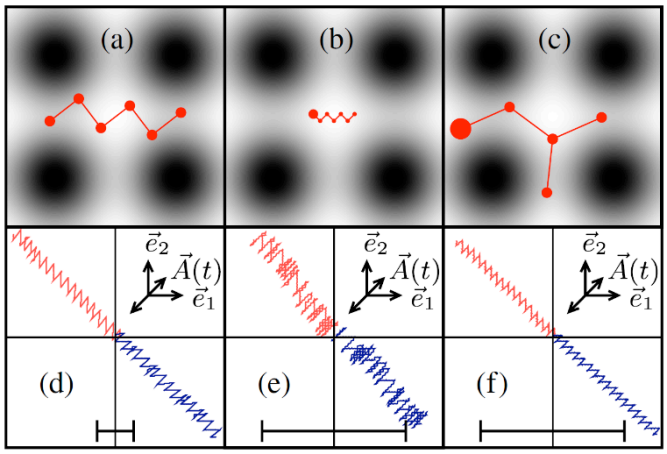

Fig. 15 Three examples of chiral molecules consisting of rigidly coupled "atoms" (red dots connected by solid lines). The shaded background represents the periodic lattice potential with identical periods along the basic directions e_1 and e_2. (d-f) Typical single particle trajectories for the molecules shown in the corresponding panels (a-c) and their chiral partners (red and blue lines). The trajectories were obtained from numerical simulations of the equations of motion, including thermal noise. The tilting of the lattice potential along the diagonal direction switches periodically between two amplitudes, indicated by the diagonal double arrows labelled $A(t)$. Note that the magnitude and the fraction of the driving period for which the two tilting forces are applied needs to be adapted to each specific chiral molecule to achieve separation in opposite directions[46]. The bars indicate 50 lattice periods. Adapted from Ref. 46 with permission from the American Physical Society.

In the theoretical work[46], Speer et al. studied the motion of small chiral "molecules'" in a two-dimensional generic lattice potential, where the size of the chiral particles is comparable to the lattice constant of the potential. As in the studies[31,37,38] described above, the chiral objects were modelled by rigidly connected component "atoms'" with different viscous friction coefficients. By numerical simulations, Speer et al.[46] demonstrated that under the influence of a static "tilting" force the two chiral partners generically move along distinct direction through the periodic surface. They discovered that the separation effect is strongest if the tilting force A is oriented along the diagonal symmetry direction of the square lattice potential, because then the two enantiomers move

Please do not adjust margins

along the two lattice directions, i.e. the e_1 and e_2 directions. Moreover, which one of the two enantiomers migrates in which direction was found to depend on the amplitude of A, such that by suitable periodic switching between different A-magnitudes (at fixed orientation) the two chiral partners could be made to move into opposite directions (see Fig. 15). This chiral separation mechanism proved to be remarkably robust against thermal noise[46].

In the experimental follow-up work[47], the two-dimensional lattice potential was realized by a square lattice of cylindrical posts in a microfluidic channel (post radius around 3 μm , lattice constant 20 μm, channel height 6 μm). As chiral test particles, Bogunovic et al.[47] used left-handed and right-handed L-shaped objects[48] with long and short ``legs'' of about 15 μm and 10 μm (see Fig. 16a).

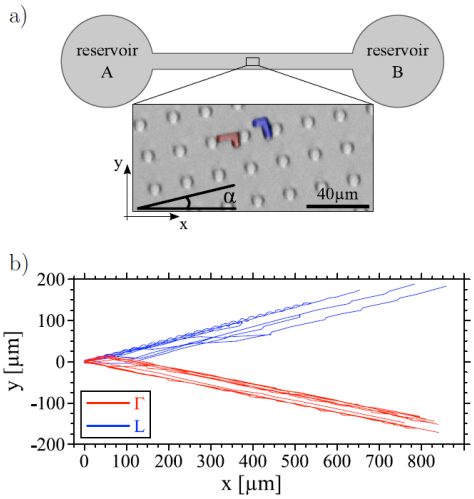

Fig. 16 a) Schematic top-view (x-y plane) of the microfluidic channel containing a periodic post array, inclined by an angle α with respect to the channel axis (x-direction). Fluid and particles can be injected into the linear channel via two reservoirs at its ends. A steady fluid flow through the channel is generated by a pressure difference applied to the two reservoirs. The magnified inset shows an optical micrograph image of the square lattice of cylindrical posts, as well as two L-shaped particles of opposite chirality coloured in blue (L particle) and red (Γ particle). b) Experimental trajectories observed in the set-up from (a) with α=15° for several of the both chiral particles from (a), demonstrating chiral separation in the post array. Adapted from Ref. 47 with permission from the American Physical Society

The dimensions of the microfluidic channel and the particles were matched, such that the chiral particles could edge through the post array without being able to rotate around their long axis and switch chirality in that way. The chiral particles were advected through the post array by a steady pressure-driven fluid flow. For this setup, Bogunovic et al.[47] performed extensive numerical simulations of a simple Brownian dynamics model to systematically investigate the net velocity and direction of motion of the enantiomers as a function of the inclination angle between the post array and the flow direction. Then, a successful experimental separation of left- and right-handed L-shaped particles was conducted for an inclination angle α=15° and a fluid flow velocity of the order of 100 μm/s, see Fig.16b.

7 Optical forces

It has been recognised in recent years that light can be used to exert discriminatory forces on chiral objects and that this might form the basis of new schemes for chiral resolution.

The earliest work on chiral optical forces seems to be a theoretical proposal put forward by Yong, Bruder and Sun in 2007.[49] These authors considered a three-level model of an 'oriented' chiral molecule, illuminated by three overlapping beams of light in a Δ-type configuration. The enantiomers of this molecule were shown to follow different trajectories in space due to their interaction with the light. The chiral discrimination here results from the cyclic nature of the Δ-type configuration (which is uniquely supported by chiral molecules, owing to their indefinite parity) together with the enantiomer-dependent signs of the Rabi frequencies that connect the three levels. Li and Shapiro presented a refined theory of this phenomenon and offered their own schemes[50,51]. It was argued shortly thereafter by Jacob and Hornberger[52], however, that such approaches are not feasibly in reality: when the rotational diffusion is accounted for, chiral discrimination is eliminated or else severely reduced. Also noteworthy is a theoretical proposal by Eilam and Shapiro[53] to spatially separate chiral homodimers from their achiral heterodimer counterparts, by preparing them in different internal states so that they experience different optical forces in a given light field. Again, rotational degrees of freedom were neglected. It is interesting that these early proposals[49–51] have elements in common with a spectroscopic technique for chiral molecules demonstrated recently by Patterson, Schnell and Doyle[54], in which three rotational levels are used to discriminate between enantiomers on the basis of the sign of the product of three transition electric-dipole moment components.

The first experimental demonstration of a chiral optical force was reported by Cipparrone and co-workers in 2011[55], foreshadowed by the theoretical work of Ross and Lakhtakia[56] as well as Guzatov and Klimov[57]. Cipparrone and co-workers showed that left-handed cholesteric liquid crystal droplets were either trapped in or expelled from optical tweezers, depending on whether the tweezers had left- or right-handed circular polarisation. This form of chiral discrimination occurs because the droplet acts as a circular Bragg reflector: left-handed light is reflected whereas right-handed light is transmitted, resulting in different optical forces. Cipparrone and co-workers also reported on anisotropic chiral microspheres, which exhibited much more exotic dynamics than their isotropic counterparts.[55] It is interesting to note that a circular Bragg reflector acts as a 'chiral mirror', reversing the spin of incident light whilst maintaining the helicity (in contrast, a conventional mirror reverses the helicity of incident light while maintaining the spin). The associated torque was observed by Donato[58], Brzobohaty[59] and Tkachenko[60] in three independent studies.

That fact that this torque could be used for chiral sorting was found independently by Tkachenko and Brasselet in 2013[61] . After which they went on to demonstrate the first optical chiral sorter.[62] Their device consisted of two counter-

This journal is © The Royal Society of Chemistry 20xx

Please do not adjust margins

propagating circularly polarised beams of light with opposite helicities. Cholesteric liquid crystal droplets of a given chirality flowing through the sorter were deflected depending on the helicities of the beams whereas achiral droplets were unaffected; see Fig. 17. It was found, moreover, that the sorter was able to deflect left- and right-handed droplets in opposite directions even when the frequency of the light was removed from the Bragg window. The (smaller) effect here was attributed to discriminatory refraction and scattering rather than Bragg reflection. Tkachenko and Brasselet concluded by proposing that the functionality of their sorter might be extended down to the nanometre (molecular) scale by exploiting functionalised chiral microparticles as 'chiral conveyers' [62].

In recent years, theoretical work has focussed on nanoscale chiral objects, including chiral molecules. Canaguier-Durand, Genet and co-workers[63] proposed a systematic description of the forces and torques that chiral light fields can exert on chiral objects. In this work, chiral objects were described in the dipolar regime and time-averaged forces and torques evaluated from the classical Lorentz law. This approach revealed a new type of force, stemming from the mechanical coupling between the electric-magnetic dipole polarizability tensor and the quantities (density and flow) that characterize the chiral content of a light field.[64] Remarkably, the reactive and dissipative components of the chiral force are determined, respectively, from the real (rotatory power) and imaginary (circular dichroism) parts of the electric- magnetic polarizability tensor of the chiral dipole. This in turn implies that the direction of the chiral optical force directly depends on the enantiomeric form of the chiral object considered, a property that gives unexpected opportunities for proposing new mechanisms for enantiomeric separation involving chiral light, both in the far and near fields[65–68] .

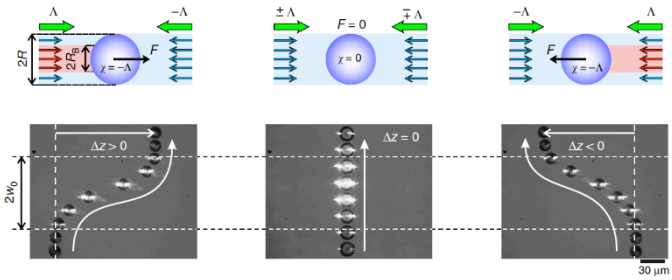

Fig. 17 A chiral optical sorter combining laminar flow with chiral optical forces. Particles can be deflected to the right or left depending on their chirality and the polarization of the light. $\chi = 0$ refers to non-chiral medium and $\chi = \pm 1$ to right/left-handed chiral media. Adapted from Ref. 60 with permission from Springer Nature.

Cameron and co-workers [69,70] explained, independently from Genet et al. [63], that a gradient in the helicity (00-zilch or 'optical chirality') of an optical field can be used to accelerate the enantiomers of a chiral molecule in opposite directions and that this 'discriminatory optical force for chiral molecules' might be exploited to spatially separate the enantiomers of chiral molecules, prepared as constituents of a dilute molecular beam. A key feature of the Cameron proposal was the use of optical beams with only a small angle between their propagation directions, which forms a helicity grating with an adjustable period[71]. It is interesting to note that the potential energy underpinning this optical force is the same as that which governs optical refraction, with the chirality sensitive contribution in particular giving rise to natural optical rotation[63,72] .

In a series of works[73–79] , Bradshaw and co-workers proposed that the same potential energy[69,70,72] might be used to significantly modify the local enantiomeric excess of chiral molecules in solution, by illuminating the solution with a circularly polarised beam of light. The viability of this scheme and the validity of the analysis was debated in two different works.[80,81]

Rukhlenko and co-workers[82] considered two counter-propagating plane waves of opposite helicity, allowing for the possibility that the waves might have different frequencies and / or intensities. Neglecting interference between the waves, these authors showed that the average optical force exerted on an isotropic chiral nanoparticle by the light field is absolutely discriminatory to leading order, for appropriate choices of the frequencies and intensities of the waves that depend in general upon the properties of the nanoparticle. The chiral discrimination here can be attributed to circular dichroism: the chiral nanoparticle absorbs photons at different rates from the two waves and so experiences a net force. For equal frequencies and intensities, this optical field is essentially that proposed by Canaguier-Durand and co-workers[63] and used by Tkachenko and Brasselet in their chiral optical sorter.[62] Rukhlenko and co-workers went on to analyse the optical force-induced diffusion in their setup and concluded that "*although the proposed method is unsuitable for the direct separation of chiral molecules, it can still be used to separate them if they are attached to chiral particles with large (chiral response)*". Again, this is reminiscent of the 'chiral conveyer' idea put forward by by Tkachenko and Brasselet[62]. Complementing such experiments, Brasselet et al.[83] have been able to selectively displace chiral liquid crystal microspheres using forces arising from optical helicity gradients, thereby implementing the classical analogue of the molecular Stern-Gerlach chiral sorter proposed by Cameron and co-workers[69,70]. Recently, Kravets[84] et al. extended experimental attempts to observe discriminatory optical forces exerted on individual chiral objects by chiral light to many-body systems, demonstrating chirality-selective mechanical separation of randomly distributed assemblies of right-handed and left-handed chiral microparticles by optical means. This work opens the way for further experimental implementation by considering particles with smaller sizes.

Progress on the first experiment aimed at measuring the discriminatory optical force for chiral molecules was reported by Jones and co-workers[85]. These authors used a Poincaré beam of light, which has a spatially varying polarisation pattern, to try to induce a measurable local enantiomeric excess in a racemic solution. They obtained a null result, attributed to the overpowering effects of diffusion and dipole optical forces.

Please do not adjust margins

To move toward manipulating chiral matter at nanometer scales, it is important to be capable of spatially controlling single chiral nano-object in freestanding conditions and, simultaneously, recognizing their enantiomeric form. Crucial steps in these directions have recently been taken, with new schemes, such as those proposed by Cheshnovsky and co-workers[86] for sensitive CD extinction measurements on individual chiral artificial nano-objects and nanocrystals. Schnoering et al. have optically trapped single metallic chiral nanopyramids that display remarkably large chiral responses[87]. Exploiting a fundamental consequence of the conservation law of optical chirality proposed by Poulikakos, Norris and co-workers[88], they developed a polarimetric setup that performs, inside the optical trap, chiral recognition of such single nano-enantiomers[87]. In this context, it is important to mention that, as demonstrated by Dionne et al.[89], chiral atomic force microscopy probes currently open new experimental paths for revealing and quantifying chiral optical forces at the nanoscale.
An aspect of chiral optical forces that requires further attention in theory is the rotational degrees of freedom. It is important to distinguish between an isotropic chiral object (considered in many theoretical studies so far) and an isotropically averaged object, resulting from anisotropic individual components, such as a chiral molecule. The optical response of a chiral molecule is strongly dependent on the molecule's orientation with respect to the light. The chiral optical force experienced by a chiral molecule will therefore differ in magnitude and sign from the isotropically averaged prediction. This subtlety should be taken into account at the single-molecule level and might even be exploited to increase the efficiency of separation. This argumentation is again similar to that made in Fig. 4: by restricting rotational diffusion chiral mechanical forces can become more directional, leading to better resolution.
Another interesting aspect is the possibility given by the chiral electric-magnetic polarizability tensor to induce linear-to-angular crossed momentum transfers. Such transfers can take various dynamical forms, from lateral and "pulling" forces[90–94] to "left-handed" optical torques[95,96]. As they are mediated by the chirality of the dipole, these forces and torques have the potential to yield new all-optical schemes to achieve molecular resolution. For this reason, these perspectives certainly deserve further study.

Conclusions

Chiral resolution of enantiomers is and will remain of eminent importance for our society. Despite established separation techniques based on, e.g., chiral column chromatography the search for new methods to achieve faster and more efficient resolution is still ongoing. Mechanical chiral resolution is a promising approach, and can be achieved using mechanical and/or optical forces as shown in this review. However, in most cases (rotational) diffusion decreases the efficiency, since the chiral forces are coupled directly to the orientation of the molecule or particle. Future strategies to lower the rotational diffusion using a secondary 'aligning field' (e.g., by applying an electric and/or magnetic field) are therefore very interesting. The theoretical understanding of mechanical resolution is steadily improving and increasingly taking into account diffusion and hydrodynamic interactions. For future theoretical studies, there is still room for improvement by including chiral particle–particle interactions for example, which will become important for industrial systems working at high concentrations. Overall, the scepticism of achieving molecular scale mechanical resolution is slowly withering, opening up avenues towards a new generation of chiral separation devices.

Conflicts of interest

There are no conflicts to declare.

Acknowledgements

AT acknowledges generous funding from Solvay, VM was partially funded through SATT Conectus Alsace. RPC gratefully acknowledges support from The Leverhulme Trust (RPG-2017-048). SMB thanks the Royal Society for the award of a Research Professorship (RP150122). RE acknowledges financial support from the Swedish Research Council (Vetenskapsrådet) under the grant No. 2016-05412. CG acknowledges Agence Nationale de la Recherche (ANR), France, ANR Equipex Union (Grant No. ANR-10-EQPX-52-01), the Labex NIE projects (Grant No. ANR-11-LABX-0058-NIE), and USIAS within the Investissements d'Avenir program (Grant No. ANR-10-IDEX-0002-02).

Notes and references

1 Plato (translation by B. Jowett), *Timaeus*, Macmillan, 1959.
2 L. Pasteur, *Recherches sur les relations qui peuvent exister entre la forme cristalline, la composition chimique et les sens de la polarisation rotatoire*, Impr. Bachelier, 1848.
3 A. J. Fresnel, H. H. de Sénarmont, E. (Émile) Verdet and L. F. Fresnel, *Œuvres complètes d'Augustin Fresnel*, Paris, Imprimerie impériale, 1866.
4 J. A. Le Bel, *Bull. soc. chim. France*, 1874, **22**, 337–347.
5 J. H. Van 't Hoff, *Archives neerlandaises des sciences exactes et naturelles*, 1874, **9**, 445–454.
6 W. T. Kelvin Baron and W. Thomson, *Baltimore Lectures on Molecular Dynamics and the Wave Theory of Light*, Cambridge University Press, 2010.
7 E. J. Ariëns, *Medicinal Research Reviews*, 1986, **6**, 451–466.
8 S. W. Smith, *Toxicol Sci*, 2009, **110**, 4–30.
9 K. Banerjee-Ghosh, O. Ben Dor, F. Tassinari, E. Capua, S. Yochelis, A. Capua, S.-H. Yang, S. S. P. Parkin, S. Sarkar, L. Kronik, L. T. Baczewski, R. Naaman and Y. Paltiel, *Science*, 2018, **360**, 1331–1334.
10 B. Sun, Y. Kim, Y. Wang, H. Wang, J. Kim, X. Liu and M. Lee, *Nature Materials*, 2018, **17**, 599.
11 D. W. Howard, E. N. Lightfoot and J. O. Hirschfelder, *AIChE Journal*, 1976, **22**, 794–798.
12 M. Tencer and R. Bielski, *Chirality*, 2011, **23**, 144–147.

 This journal is © The Royal Society of Chemistry 20xx

13 A. Einstein, *Investigations on the Theory of the Brownian Movement*, Courier Corporation, 1956.
14 M. Smoluchowski, *Essai d'une théorie cinétique du mouvement Brownien et des milieux troublés*, Acad. Litterarum Cracoviensis, 1906.
15 P. Curie, *J. Phys. Theor. Appl.*, 1894, **3**, 393–415.
16 L. D. Barron, *Chem. Soc. Rev.*, 1986, **15**, 189–223.
17 C. Welch, *Enantiomer*, 1998, **3**, 275–281.
18 P. G. de Gennes, *EPL*, 1999, **46**, 827.
19 J. Lever, *Basteria*, 1958, **22**, 21–51.
20 B. Pasteur, in *Annales de chimie et de physique*, G. Masson, Paris, 1890, pp. 433–510.
21 Y.-J. Kim and W. J. Rae, *International Journal of Multiphase Flow*, 1991, **17**, 717–744.
22 M. Makino and M. Doi, *Physics of Fluids*, 2005, **17**, 103605.
23 T. M. Hermans, K. J. M. Bishop, P. S. Stewart, S. H. Davis and B. A. Grzybowski, *Nature Communications*, 2015, **6**, 5640.
24 M. Makino, L. Arai and M. Doi, *J. Phys. Soc. Jpn.*, 2008, **77**, 064404.
25 N. B. Baranova and B. Ya. Zel'dovich, *Chemical Physics Letters*, 1978, **57**, 435–437.
26 D. Schamel, M. Pfeifer, J. G. Gibbs, B. Miksch, A. G. Mark and P. Fischer, *J. Am. Chem. Soc.*, 2013, **135**, 12353–12359.
27 J. B. Clemens, O. Kibar and M. Chachisvilis, *Nature Communications*, 2015, **6**, 7868.
28 G. M. Whitesides, *Nature*, 2006, **442**, 368–373.
29 D. Belder and M. Ludwig, *Electrophoresis*, 2003, **24**, 2422–2430.
30 S. Nagl, P. Schulze, M. Ludwig and D. Belder, *Electrophoresis*, 2009, **30**, 2765–2772.
31 M. Kostur, M. Schindler, P. Talkner and P. Hänggi, *Phys. Rev. Lett.*, 2006, **96**, 014502.
32 S. Burger, T. Franke, T. Fraunholz, R. H. W. Hoppe, M. A. Peter and A. Wixforth, *Computational Methods in Applied Mathematics*, 2015, **15**, 247–258.
33 K. Beleke-Maxwell, T. Franke, R. H. W. Hoppe and C. Linsenmann, *Computers & Fluids*, 2015, **112**, 50–60.
34 Z. Guttenberg, A. Rathgeber, S. Keller, J. O. Rädler, A. Wixforth, M. Kostur, M. Schindler and P. Talkner, *Phys. Rev. E*, 2004, **70**, 056311.
35 N. Watari and R. G. Larson, *Phys. Rev. Lett.*, 2009, **102**, 246001.
36 P. Talkner, G.-L. Ingold and P. Hänggi, *New J. Phys.*, 2012, **14**, 073006.
37 R. Eichhorn, *Phys. Rev. Lett.*, 2010, **105**, 034502.
38 R. Eichhorn, *Chemical Physics*, 2010, **375**, 568–577.
39 S. Meinhardt, J. Smiatek, R. Eichhorn and F. Schmid, *Phys. Rev. Lett.*, 2012, **108**, 214504.
40 Marcos, H. C. Fu, T. R. Powers and R. Stocker, *Phys. Rev. Lett.*, 2009, **102**, 158103.
41 M. Aristov, R. Eichhorn and C. Bechinger, *Soft Matter*, 2013, **9**, 2525–2530.
42 C. K. Batchelor, *An Introduction to Fluid Dynamics*, Cambridge University Press, 1967.
43 L. Bogunovic, C. Vosskötter and D. Anselmetti, *J. Micromech. Microeng.*, 2014, **24**, 077001.
44 P. Español and P. B. Warren, *J. Chem. Phys.*, 2017, **146**, 150901.
45 A. D. Stroock, S. K. W. Dertinger, A. Ajdari, I. Mezić, H. A. Stone and G. M. Whitesides, *Science*, 2002, **295**, 647–651.
46 D. Speer, R. Eichhorn and P. Reimann, *Phys. Rev. Lett.*, 2010, **105**, 090602.
47 L. Bogunovic, M. Fliedner, R. Eichhorn, S. Wegener, J. Regtmeier, D. Anselmetti and P. Reimann, *Phys. Rev. Lett.*, 2012, **109**, 100603.
48 L. Bogunovic, D. Anselmetti and J. Regtmeier, *J. Micromech. Microeng.*, 2011, **21**, 027003.
49 Y. Li, C. Bruder and C. P. Sun, *Phys. Rev. Lett.*, 2007, **99**, 130403.
50 X. Li and M. Shapiro, *J. Chem. Phys.*, 2010, **132**, 041101.
51 X. Li and M. Shapiro, *J. Chem. Phys.*, 2010, **132**, 194315.
52 A. Jacob and K. Hornberger, *J. Chem. Phys.*, 2012, **137**, 044313.
53 A. Eilam and M. Shapiro, *Phys. Rev. Lett.*, 2013, **110**, 213004.
54 D. Patterson, M. Schnell and J. M. Doyle, *Nature*, 2013, **497**, 475–477.
55 G. Cipparrone, A. Mazzulla, A. Pane, R. J. Hernandez and R. Bartolino, *Advanced Materials*, 2011, **23**, 5773–5778.
56 B. M. Ross and A. Lakhtakia, *Optik*, 2008, **119**, 7–12.
57 D. V. Guzatov and V. V. Klimov, *Quantum Electron.*, 2011, **41**, 526.
58 M. G. Donato, J. Hernandez, A. Mazzulla, C. Provenzano, R. Saija, R. Sayed, S. Vasi, A. Magazzù, P. Pagliusi, R. Bartolino, P. G. Gucciardi, O. M. Maragò and G. Cipparrone, *Nat Commun*, 2014, **5**, 3656.
59 O. Brzobohatý, R. J. Hernández, S. Simpson, A. Mazzulla, G. Cipparrone and P. Zemánek, *Opt. Express*, 2016, **24**, 26382.
60 G. Tkachenko, M. Rafayelyan and E. Brasselet, *Phys. Rev. A*, 2017, **95**, 053839.
61 G. Tkachenko and E. Brasselet, *Phys. Rev. Lett.*, 2013, **111**, 033605.
62 G. Tkachenko and E. Brasselet, *Nature Communications*, 2014, **5**, 3577.
63 A. Canaguier-Durand, J. A. Hutchison, C. Genet and T. W. Ebbesen, *New J. Phys.*, 2013, **15**, 123037.
64 K. Y. Bliokh and F. Nori, *Phys. Rev. A*, 2011, **83**, 021803.
65 A. Canaguier-Durand and C. Genet, *Phys. Rev. A*, 2014, **90**, 023842.
66 M. H. Alizadeh and B. M. Reinhard, *ACS Photonics*, 2015, **2**, 361–368.
67 Y. Zhao, A. A. E. Saleh and J. A. Dionne, *ACS Photonics*, 2016, **3**, 304–309.
68 M. H. Alizadeh and B. M. Reinhard, *Opt. Lett., OL*, 2016, **41**, 4735–4738.
69 R. P. Cameron, A. M. Yao and S. M. Barnett, *J. Phys. Chem. A*, 2014, **118**, 3472–3478.
70 R. P. Cameron, S. M. Barnett and A. M. Yao, *New J. Phys.*, 2014, **16**, 013020.
71 R. P. Cameron, S. M. Barnett and A. M. Yao, *Journal of Modern Optics*, 2014, **61**, 25–31.
72 R. P. Cameron, PhD, University of Glasgow, 2014.
73 D. S. Bradshaw and D. L. Andrews, *New J. Phys.*, 2014, **16**, 103021.
74 D. S. Bradshaw and D. L. Andrews, *Opt. Lett., OL*, 2015, **40**, 677–680.
75 D. L. Andrews and D. S. Bradshaw, in *Complex Light and Optical Forces IX*, International Society for Optics and Photonics, 2015, vol. 9379, p. 93790Q.
76 D. S. Bradshaw and D. L. Andrews, *J. Opt. Soc. Am. B, JOSAB*, 2015, **32**, B25–B31.
77 D. S. Bradshaw, J. M. Leeder, M. M. Coles and D. L. Andrews, *Chemical Physics Letters*, 2015, **626**, 106–110.
78 D. S. Bradshaw, K. A. Forbes, J. M. Leeder and D. L. Andrews, *Photonics*, 2015, **2**, 483–497.
79 D. S. Bradshaw and D. L. Andrews, in *Complex Light and Optical Forces X*, International Society for Optics and Photonics, 2016, vol. 9764, p. 97640W.
80 D. S. Bradshaw, M. M. Coles and D. L. Andrews, *arXiv:1507.04231 [physics],2015*.

This journal is © The Royal Society of Chemistry 20xx

Please do not adjust margins

81 R. P. Cameron, S. M. Barnett and A. M. Yao, *arXiv:1506.07423 [physics],2015*.
82 I. D. Rukhlenko, N. V. Tepliakov, A. S. Baimuratov, S. A. Andronaki, Y. K. Gun'ko, A. V. Baranov and A. V. Fedorov, *Scientific Reports*, 2016, **6**, 36884.
83 N. Kravets, A. Aleksanyan and E. Brasselet, *Phys. Rev. Lett.*, 2019, **122**, 024301.
84 N. Kravets, A. Aleksanyan, H. Chraïbi, J. Leng and E. Brasselet, *Phys. Rev. Applied*, 2019, **11**, 044025.
85 J. A. Jones, B. Regan, J. Painter, J. Mills, I. Dutta, B. Khajavi and E. J. Galvez, in *Complex Light and Optical Forces XI*, International Society for Optics and Photonics, 2017, vol. 10120, p. 101200M.
86 E. Vinegrad, D. Vestler, A. Ben-Moshe, A. R. Barnea, G. Markovich and O. Cheshnovsky, *ACS Photonics*, 2018, **5**, 2151–2159.
87 G. Schnoering, L. V. Poulikakos, Y. Rosales-Cabara, A. Canaguier-Durand, D. J. Norris and C. Genet, *Phys. Rev. Lett.*, 2018, **121**, 023902.
88 L. V. Poulikakos, P. Gutsche, K. M. McPeak, S. Burger, J. Niegemann, C. Hafner and D. J. Norris, *ACS Photonics*, 2016, **3**, 1619–1625.
89 Y. Zhao, A. A. E. Saleh, M. A. van de Haar, B. Baum, J. A. Briggs, A. Lay, O. A. Reyes-Becerra and J. A. Dionne, *Nat Nanotechnol*, 2017, **12**, 1055–1059.
90 S. Sukhov and A. Dogariu, *Opt. Lett.*, 2010, **35**, 3847.
91 S. B. Wang and C. T. Chan, *Nature Communications*, 2014, **5**, 3307.
92 A. Hayat, J. P. B. Mueller and F. Capasso, *PNAS*, 2015, **112**, 13190–13194.
93 M. H. Alizadeh and B. M. Reinhard, *ACS Photonics*, 2015, **2**, 1780–1788.
94 A. Canaguier-Durand and C. Genet, *Phys. Rev. A*, 2015, **92**, 043823.
95 D. Hakobyan and E. Brasselet, *Nature Photon*, 2014, **8**, 610–614.
96 A. Canaguier-Durand and C. Genet, *J. Opt.*, 2015, **18**, 015007.

This journal is © The Royal Society of Chemistry 20xx